Cerebral Cortex July 2008;18:1588–1603
doi:10.1093/cercor/bhm189
Advance Access publication November 12, 2007

Critical Period Plasticity of Axonal Arbors of Layer 2/3 Pyramidal Neurons in Rat Somatosensory Cortex: Layer-Specific Reduction of Projections into Deprived Cortical Columns

P. Broser[1], V. Grinevich[2,3], P. Osten[2,3], B. Sakmann[1] and D.J. Wallace[1]

[1]Department of Cell Physiology, [2]Department of Molecular Neurobiology, Max Planck Institute for Medical Research, Jahnstrasse 29, 69120 Heidelberg, Germany and [3]Department of Physiology, Feinberg School of Medicine, Northwestern University, 303 E Chicago Ave., Chicago, IL 60611, USA

We examined the effect of whisker trimming during early postnatal development on the morphology of axonal arbors in rat somatosensory cortex. Axonal arbors from populations of layer 2/3 pyramidal neurons in the D2 column were labeled by lentivirus-mediated expression of green fluorescent protein. Axonal projection patterns were compared between untrimmed control animals and animals with all whiskers in A-, B-, and C-rows trimmed (D- and E-rows left intact) from postnatal days 7 to 15 (termed from here on DE-pairing). Control animals had approximately symmetrical horizontal projections toward C- and E-row columns in both supra- and infragranular layers. Following DE-pairing, the density of axons in supragranular layers projecting from the labeled neurons in the D2 column was higher in E- than in C-row columns. This asymmetry resulted primarily from a reduction in projection density toward the deprived C-row columns. In contrast, no change was observed in infragranular layers. The results indicate that DE-pairing during early postnatal development results in reduced axonal projection from nondeprived into deprived columns and that cortical neurons are capable of structural rearrangements at subsets of their axonal arbors.

Keywords: axon anatomy, barrel cortex, extended focus imaging bright field microscopy, lentivirus, whisker

Introduction

Neurons in cortical layer 2/3 typically extend horizontally projecting axons that connect neighboring cortical areas (Gilbert and Wiesel 1979; Livingstone and Hubel 1983, 1984; Martin and Whitteridge 1984; Callaway and Katz 1990; Kenan-Vaknin et al. 1992; Yoshioka et al. 1992; Lund et al. 1993; Durack and Katz 1996; Galuske and Singer 1996; Gonzalez-Burgos et al. 2000; Miller et al. 2001; Stettler et al. 2002; Brecht et al. 2003; Petersen et al. 2003; Tanigawa et al. 2005). These connections tend to link areas that share some degree of commonality of input or response properties. For example, in monkey, cat, and ferret visual cortex, layer 2/3 axonal projections form distinct and obvious clusters where their projecting axons branch extensively (Gilbert and Wiesel 1979, 1983; Rockland and Lund 1983; Callaway and Katz 1990; Yoshioka et al. 1992; Lund et al. 1993; Levitt et al. 1994; Durack and Katz 1996; Galuske and Singer 1996; Stettler et al. 2002), and these clusters coincide with cortical columns sharing the same or similar object orientation preference (Gilbert and Wiesel 1989; Chapman and Stryker 1993; Chapman et al. 1996; Stettler et al. 2002). Further, the development of these horizontal projections is typically quite sensitive to manipulations that alter the activity of their afferent pathways (Callaway and Katz 1991; Trachtenberg and Stryker 2001).

In the rodent barrel cortex, the primary somatosensory representation of the animals facial whiskers, neurons in layer 2/3 have extensive horizontal projections into neighboring areas, both within and outside the primary somatosensory area (Miller et al. 2001; Brecht et al. 2003; Hoffer et al. 2003, 2005; Hoover et al. 2003; Petersen et al. 2003). Within the barrel cortex itself layer 2/3 neurons have dense projections into neighboring columns. Consistent with this axonal anatomy, studies in acute brain slices show that electrical stimulation in a layer 4 barrel elicits responses that spread into layer 2/3 in a columnar fashion, before spreading horizontally in layer 2/3 and additionally into deeper layers of surrounding columns (Petersen and Sakmann 2001; Wirth and Luscher 2004). Analyses of response latencies in layer 2/3 neurons in vivo following deflections of single whiskers suggest that activity also spreads horizontally from the column associated with the stimulated whisker into its surrounding columns (Armstrong-James et al. 1992; Brecht et al. 2003). More recently, studies using voltage-sensitive dyes (vsd) have demonstrated that responses in layer 2/3 are initially restricted to an area approximately bounded by the dimensions of the layer 4 barrel topographically aligned to the deflected whisker and then spread horizontally into neighboring columns in all directions (Petersen et al. 2003; Wallace and Sakmann 2007). Perhaps not surprisingly, the spread of the vsd signal after stimulation of a single whisker bears remarkable similarity to the population axonal projection pattern observed after bulk labeling of layer 2/3 neurons (Miller et al. 2001; Petersen et al. 2003).

Barrel cortex has also been shown to be highly malleable (Simons and Land 1987; Fox 1992; Glazewski and Fox 1996; Glazewski et al. 1998; Polley et al. 1999; Feldman and Brecht 2005). Sensory deprivation brought about by trimming of whiskers can cause alterations in the cortical representation of both the trimmed and nontrimmed whiskers. This plasticity can be manifested, for example, as a decrease in the responsiveness of individual neurons in the deprived columns, that is, those representing the trimmed whiskers, or as an increase in responsiveness in nondeprived columns (Fox 1992; Glazewski and Fox 1996; Glazewski et al. 1998). It has been shown, using vsd-imaging, that the spatiotemporal dynamics of the spread of activity in layer 2/3 are sensitive during early postnatal development to manipulations influencing afferent sensory signals (Wallace and Sakmann 2007). This study showed that pairing of D- and E-rows of whiskers (i.e., trimming of A-, B- and C-rows, referred to from here on as DE-pairing) during early postnatal development causes a change in the response to deflection of D-row whiskers. Specifically, activity spreading through layer 2/3 away from an activated D-row column is changed from being roughly symmetrical in animals with all

whiskers intact to being asymmetrical with a bias in spread toward the nondeprived E-row columns after DE-pairing. Because first the projection pattern of layer 2/3 axons spreading horizontally around individual cortical columns in barrel cortex show similarity to the shape of the spreading vsd signal (Miller et al. 2001; Petersen et al. 2003; Wallace and Sakmann 2007), and second horizontal axonal projections in layer 2/3 of developing visual cortex show rapid structural modification in response to alterations in sensory input (Trachtenberg and Stryker 2001), we hypothesized that the changes in the vsd signal induced by DE-pairing described above result from alterations in the horizontal axonal projections of the layer 2/3 pyramidal cells. To investigate this hypothesis, we used a technique recently developed for quantification of axonal projections from populations of labeled neurons (P. J. Broser et al., submitted for publication). This technique allows quantification of the summed length of axonal arbors in user-defined regions of interest around a population of labeled cells. Here we made injections of a lentiviral construct expressing enhanced green fluorescent protein to selectively label populations of layer 2/3 pyramidal neurons and investigated whether the characteristics of the axonal projection pattern emanating from these cells is altered after DE-pairing. The axonal arborizations of the layer 2/3 neurons branched extensively both in layer 2/3 and in layer 5 of the surrounding cortical areas. Within layer 2/3, we found that DE-pairing altered the balance of the axonal projection pattern, resulting in a higher projection density over the nondeprived E-row territories. We propose that this effect results principally from a reduction in the density of the projection toward the deprived cortical columns. Surprisingly, there was no significant influence of the period of sensory deprivation on the arborizations of these same cells in infragranular layers. These results provide a plausible mechanism through which the functional changes observed after DE-pairing may occur (Wallace and Sakmann 2007) and in addition indicate that cortical pyramidal neurons may have the capacity for independent modifications at subsections of their axonal arbors on a target specific basis.

Materials and Methods

Lentivirus Preparation

Lentiviruses were produced as previously described using the FCK(1.3)GW vector containing a 1.3-kb recombinant promoter of the mouse alpha-calcium/calmodulin-dependent protein kinase II (α-CaMKII) gene (Dittgen et al. 2004); this promoter drives expression specifically in pyramidal neurons (the vector backbone is based on a construct FUGW, described in Lois et al. 2002). The titer of the injected virus was in the range of 5×10^5 to 1×10^6 infectious particles per microliter.

Animals, Surgery, and Virus Injections

Experimental animals were Wistar rats of either sex. All animal procedures were conducted according to the guidelines of the Max Planck Society. Sensory deprivation (DE-pairing) involved daily trimming of the whiskers from postnatal days (p) 7 to 17 and subsequently from the day of the injection until the animals were sacrificed. The rat pups were gently held and all whiskers in rows A, B, and C as well as the alpha, beta, and gamma whiskers were trimmed to the level of the facial fur. Control animals were littermates of the trimmed animals and were handled in the same way and for approximately the same amount of time. Animals remained with their mother until the time of the injection, after which they were each individually housed.

Lentivirus injections into primary somatosensory cortex were made in the control and DE-paired animals at around p18 and were targeted to the cortical column representing the D2 whisker by optical intrinsic signal imaging (see below). The rat pups were anesthetized by intraperitoneal injection of Nembutal (sodium pentobarbital, 50 mg/kg). Anesthetic state was monitored throughout the procedure via testing of paw withdrawal and corneal reflexes with supplementary doses of Nembutal (5 mg/kg) given as necessary. The skull over the left primary somatosensory whisker representation was exposed and an approximately 3 × 3-mm area of bone centered at 2.5 mm posterior to and 5 mm lateral to bregma was thinned until it was transparent when covered with saline solution. Optical intrinsic signal responses to stimulation of the D2 whisker were then acquired through the thinned skull using standard intrinsic imaging techniques (excitation illumination 630 ± 15 nm, frame rate 100 ms per frame; Grinvald et al. 1986; Ratzlaff and Grinvald 1991). After identifying the cortical representation of the D2 whisker, a small craniotomy (approximately 300 × 300 μm) was made over the responsive area of cortex and the dura opened. Great care was taken throughout this procedure to avoid damage to the underlying cortical surface. An injection pipette (tip opening approximately 7–9 μm) was then advanced into the cortex taking care to ensure that the orientation of the pipettes advance was perpendicular to the pial surface. Approximately, 100 nL of the viral stock solution was then slowly injected into layer 2/3 at approximately 400 μm below the pia. The skin incision was then closed with silk sutures and the animals allowed to recover with free access to food and water.

Histology

After a period of 10–20 days to allow adequate viral expression, animals were deeply anesthetized with isoflurane and then perfused transcardially first with phosphate buffer (pH 7.2) and subsequently with 4% paraformaldehyde in phosphate buffer. The brain was removed and postfixed in the paraformaldehyde solution overnight at 4 °C. Fifty- or 100-μm-thick tangential sections were then cut from the injected hemisphere using a vibratome (50-μm sections from 5 control and 5 DE-paired animals; 100-μm sections from 3 control and 2 DE-paired animals).

After washing in phosphate-buffered saline (PBS, pH 7.4, 3 × 10 min) sections were preincubated in 1% H_2O_2 in PBS for 1 h at room temperature (RT). Sections were then extensively washed with PBS (6 × 10 min) and were preincubated in 10% normal goat serum (NGS, Sigma-Aldrich, St. Lois, MO) diluted in 1% Triton-X100 solution in PBS for 2 h at RT. Sections were then incubated overnight with primary rabbit polyclonal antibodies against green fluorescent protein (GFP, 1:10 000, Invitrogen/Molecular Probes, CA) in working solution (1% NGS, 0.5% Triton in PBS) at RT. Next morning sections were washed in PBS (3 × 10 min) and incubated with biotinylated goat anti-rabbit IgG (Vector Elite kit, Vector Laboratories, Inc., Burlingame, CA; 1:500) for 2 h at RT. After washing in PBS, avidin:biotinylated horseradish peroxidase complex (Vectastain ABC kit, Vector Laboratories, CA) in PBS was applied for 1 h at RT. Immunolabeling was revealed by the glucose oxidase–diaminobenzidine (GOD–DAB) method described by Zaborsky and Heimer (1989). Intensification of the immunoreaction product was carried out using nickel-intensification of the GOD–DAB reaction product (Liposits et al. 1986; Zaborsky and Heimer 1989). After extensive washing in PBS, sections were mounted on Superfrost (Menzel, Braunschweig, Germany) glass slides, dried, dehydrated through ascending concentrations of ethanol, cleared in xylol, and mounted with embedding medium (Eukitt, Sigma-Aldrich, St. Lois, MO).

MEFI Microscopy, Automated Axon Length Quantification and Analysis Pinwheels

To quantify the axonal projections we used the technique of mosaic extended focus imaging (MEFI) microscopy and automated axon quantification described by (P. J. Broser et al., submitted for publication). Briefly, high spatial resolution images of the 3 × 3-mm area around the injection site were acquired using a 20× objective and MEFI microscopy. All axonal processes in these images were traced and the total length of traced axon was quantified, with both steps using custom written image-processing software specifically developed for

quantification of axonal processes from bulk labeled populations of neurons (P. J. Broser et al., submitted for publication). To quantify the radial spread of axonal processes around the injection site we used a polar measurement grid referred to from here on as a "pinwheel." The origin of the pinwheel was located on the center of the injection site, and the zero degree or "D-row axis" was aligned to a straight line connecting the center of the injection site and the center of the D3 barrel (see Supplementary Fig. S1). The location of the center of the D3 barrel was established from cytochrome oxidase–stained sections in layer 4. As all our injections were made approximately in the center of the D2 column, the orientation of the pinwheel was approximately aligned to the D-row axis. Placement of the pinwheel on all supra- and infragranular sections was achieved using radial blood vessels as fiducial landmarks (see Supplementary Fig. S1*B*,*C*). The maximum radius of the pinwheel was 1050 μm. Each element in the pinwheel was 50 μm wide and subtended an angle of 15°, with the total length of axon in each element of the grid being quantified. For initial analyses, the total length of axon in each element was normalized to the area of the element to yield a map of axonal density (Supplementary Fig. S1*E*). The total axonal length within subregions of these density maps could then be further compared by defining regions of interest comprising a user-defined number of individual elements at any location of the map.

Data Inclusion Criteria and Exclusion Zones

The criteria for inclusion of any experiment in the data set to be analyzed were 1) the center of the injection site in layer 2/3 had to be within the boundary of the D2 barrel column as reconstructed from cytochrome oxidase-stained layer 4 sections, 2) the majority of the labeled somas fell within the area bordered by the D2 barrel as described in 1 above, and 3) the cutting angle had to be approximately tangential over the C, D, and E columns as defined by the ability to visualize cytochrome-stained barrels representing columns in arcs 1–3 of all 3 of these rows in a single layer 4 section.

For analysis purposes here, supragranular sections were defined as all sections above the first section in which barrels in the first 3 arcs of C-, D-, or E-row were visible. Similarly, infragranular sections were defined as all sections below the last section in which the barrels mentioned above were visible.

We also established the following criteria for the inclusion of any individual section from a single experiment into the data set to be analyzed: 1) the distance from the center of the injection site to the edge of the section had to be at least 750 μm, and 2) the section had to be free of damage or irregularities in the area to be analyzed.

Finally, the density of the labeled neuronal processes around the center of the injection site was so high that accurate tracking of individual processes was not possible. This area also contains the highest density of labeled dendrites (Brecht et al. 2003). We therefore excluded a circular zone with a radius of 250 μm from the center of the injection site from all analyses.

Decisions regarding the inclusion of any experiment into the data set to be analyzed, as well as decisions on which sections from any individual experiment to analyze and the placement and orientation of the analysis pinwheel on all sections analyzed from any given experiment were all made with the investigator blind to the experimental condition of the particular experiment under consideration.

Analyses

In order to minimize artifacts relating to variations in cutting angle, axonal lengths, for both supra- and infragranular regions, were quantified in as many adjacent serial sections as met the above inclusion criteria. This involved first quantifying axonal lengths within the analysis pinwheel in all sections to be included in the analysis of a given laminar region (e.g., supragranular or infragranular) for a given animal, and then summing these pinwheels (element wise) to give the "summed analysis pinwheels" used for subsequent analyses.

C- and E-Row Analysis Regions

For initial analysis we defined the angular limits of C- and E-row facing regions of interest as follows: C-row region, 0–180°; E-row region, 180–360°. Radial dimensions in both cases were 250–750 μm.

Analysis Quadrants

For a more refined spatial analysis we defined 4 quadrant regions of interest as follows: Quadrant 1, 15–90°; Quadrant 2, 90–165°; Quadrant 3, 195–270°; Quadrant 4, 270–345°. Radial dimensions for all quadrants were 250–750 μm.

Supra- and Infragranular Ratiometric Analyses

Single summed analysis pinwheels were calculated for each animal in either supra- or infragranular regions as described above. Subsequently, the total axonal load in each quadrant or row region was calculated by summing the axonal lengths in all elements within each individual quadrant or region. Ratios between all quadrants or regions were then calculated, resulting in a single ratio for each pair of quadrants and for the row regions for each animal.

Three-dimensional Contours

To more precisely visualize and compare the projection patterns across all cortical layers together, we developed a method for generating a three-dimensional (3D) contour. In effect, these contours represent a unique 3D shape enclosing a user-defined percentage of the total summed length of all detected axons.

The 3D contour was determined using an iterative bidisection algorithm. This algorithm starts with a preset threshold (typically the total axonal load in all pinwheels) and a target percentage. The algorithm then calculates the 3D contour enclosing the target percentage of the total summed length of axons in all sections over which the contour was to be calculated. For the contours calculated here we used a total of 21 sections, covering a radial thickness of cortex from approximately 250 μm above the top of the barrels in layer 4 to approximately 800 μm below this point (see below for further details). Each iteration of the algorithm had 2 steps. In the first step, an estimated 3D contour was calculated and the total axonal load contained with the contour measured. This first step, in turn, consisted of the following 3 steps: 1) for the pinwheels from each of the sections to be included in the 3D contour, the threshold value was used to generate an isoline outside of which the threshold length of axon resided. These isolines were calculated by summing the total axonal load along each 15° radial section from the outermost element to the innermost and locating the position where the threshold was most closely met. 2) The total axonal load contained within the isoline was calculated for each pinwheel. 3) The total axonal load for the estimated 3D contour was then calculated by summing the loads calculated for each of the pinwheels. In the second step of each iteration, the threshold used for calculating the individual isolines was adjusted according to whether the total axonal load contained within the 3D contour was greater or less than the required target percentage. Iterations continued until the target percentage was found with a precision of 2%. For the contours and volume analysis done here we used a target percentage of 60%.

The fractional contour volume analyses was done by calculating for each animal the volume enclosed by the isosurface within each of the quadrants or row regions and dividing this by the total volume of the isosurface.

For display and visualization, average isosurfaces were calculated by computing the average volume of the control 3D contours. The volume of all individual 3D contours (paired and control) was uniformly scaled to the mean control volume so that all 3D contours had the same volume (the volume of the individual 3D contours being influenced by the quality of the neuronal labeling). The volume-normalized 3D contours were then averaged by taking the median of each data point of the surface of each animal. 3D contours and barrel patterns (see below) were visualized using Amira software (Mercury Computer Systems, MA). All volume analyses and statistical comparisons using the 3D contours were done on the original unscaled contours.

To ensure that the 3D contours for each animal spanned the same range of depths through the cortical layers, we used the top of the layer 4 barrels as a depth origin. We defined the section containing top of layer 4 as the first section in which barrels in each of C-, D-, and E-rows were visible. We then used a range of sections spanning 5 sections above this section to 15 sections below this section (approximately 250 μm above the top of layer 4 to 800 μm below the top of layer 4). To

generate comparable contours for both the data set using 50 μm-thick sections and the data set using 100 μm-thick sections, data for each 100 μm-thick section were repeated once. That is, the data from the first section in a 100 μm data set were used for the equivalent of sections 1 and 2 of a 50 μm data set, data from section 2 used for the equivalent of sections 3 and 4, etc.

Analysis of Injection Site Locations

Analysis of the location of injection site centers within the D2 column was conducted to test for effects of proximity of the injection site centers to the C- or E-row on the measured symmetry of the axonal projection pattern. This was done by first reconstructing the barrel pattern for each animal from cytochrome oxidase–stained layer 4 sections. A stack of images of all sections from those in layer 4 in which the barrel pattern was reconstructed to those in layer 2/3 that contained the injection site itself was made and aligned using radial blood vessels as fiducial landmarks. The location of the center of the injection site was marked in layer 2/3, and the aligned stack then used to plot its approximate position on the reconstructed layer 4 barrel pattern.

The D2 barrel was difficult to accurately reconstruct in several animals as a consequence of the dense descending axonal projection passing through layer 4 from the labeled layer 2/3 neurons. We therefore defined a "C-row line" to use as an origin for measurements of the location of the injection sites along the arc-axis (i.e., the axis connecting the C2, D2, and E2 columns). The C-row line was defined, for each animal, as a line connecting the centers of the C2 and C3 barrels. The distance to the C-row line for each injection site was then measured along a straight line running perpendicular to the C-row line. For each injection site we also determined a "D-row spread," which was designed to be a measure of the distribution of injection site locations in the row-axis (i.e., the axis connecting the D1, D2, and D3 columns). The D-row spread was defined as the distance between the center of the C2 barrel and the intersection of the C-row line and a straight line running perpendicular to the C-row line and connecting it to the injection site center.

Barrel Patterns

Two-dimensional outlines of the layer 4 barrel pattern were reconstructed for each animal from cytochrome oxidase–stained layer 4 sections. Average barrel patterns were then calculated from the individual reconstructions for both control and paired groups. The 3D barrel pattern shown in Figure 9 was created using the 2 dimensional outlines from the control group to provide the shape of the barrels and setting the height of each barrel to an arbitrary 400 μm.

Statistics

All statistical comparisons were done using Mann–Whitney *U* tests.

Many of the statistical comparisons made here required correction for multiple comparisons. As the functional changes resulting from the DE-pairing protocol, although significant, are relatively subtle (in the order of 5–10%; Wallace and Sakmann 2007), we assumed that any alterations to the axonal arbors of neurons in layer 2/3 that may in part cause these functional changes would also be relatively subtle, particularly given that the axonal arbors of layer 2/3 neurons are extensive and complex (Miller et al. 2001; Brecht et al. 2003; Larsen and Callaway 2006) and may be modified on selective branches only, or alternatively that only the axonal arbors of specific subsets of neurons may be susceptible to modification. Consequently we chose to control for multiple comparisons using the Benjamini and Hochberg method for controlling the false discovery rate (FDR, Benjamini and Hochberg 1995), because it provides considerably improved statistical power when compared with the more conservative control of family wise error rate as applied by the Bonferroni method. For the information of the reader, the adjusted alpha level using Bonferroni correction for the multiple comparisons tests performed here would be 0.0125. The FDR was controlled here at a level of 5%.

In brief, the Benjamini and Hochberg correction involves ordering according to magnitude the uncorrected *P* values for all comparisons in a given statistical analysis (in our case all *P* values generated for any individual comparison involving the defined measurement quadrants). Let P_1 be the smallest *P* value and P_4 the largest. Each *P* value is tested for

$$P_i < i/4 \times 0.05. \quad (1)$$

Let k be the largest value of i for which equation (1) holds, then reject all null hypotheses $i = 1 \ldots k$ (Benjamini and Hochberg 1995). As all statistical analyses made here that require correction for multiple comparisons involved 4 individual comparisons, the 4 critical values applying were 0.0125, 0.025, 0.0375, and 0.05. Wherever stated, *P* values refer to double-sided *P* values. Statistics given within the text are mean ± standard error and median. "*n*" values refer to number of experimental animals used.

Results

Axonal Projection Patterns from Bulk Labeling of Layer 2/3 Pyramids

We examined axonal projections from populations of layer 2/3 pyramidal neurons labeled with GFP via lentivirus-mediated gene transfer. Injections were made approximately 400 μm below the pia in the D2 column of left somatosensory barrel cortex and typically labeled populations of 200 to 400 layer 2/3 neurons. Figure 1*A* shows a coronal section through the center of a population of labeled cells. Long range axonal projections, including projections to the contralateral hemisphere, were clearly visible. Labeled layer 2/3 neurons typically had dense horizontal projections in both supragranular and infragranular layers, resulting in a characteristic "butterfly" or "hourglass" appearance in coronal and thalamocortical sections. In contrast there was almost no horizontal projection in layer 4, consistent with previous observations of axonal arborizations of individual layer 2/3 neurons (Brecht et al. 2003; Bureau et al. 2004). The primary aim of the current study was to examine whether the axonal projections of layer 2/3 pyramids in the D2 column that extend into neighboring C- or E-row territories were influenced by the DE-pairing whisker trimming protocol. We therefore analyzed horizontal projections from the labeled neurons in tangential sections from layer 2/3 and layer 5.

Alteration in Axonal Projection Patterns in Supragranular Layers by DE-Pairing

Representative examples of the axonal projection pattern in layer 2/3 from a control and DE-paired animal are shown in Figure 2*A* and *B*, respectively. The labeled layer 2/3 pyramids invariably had dense projections in supragranular layers extending in all directions from the injected D2 column into surrounding columns. In the case of the control animal, the projection from D2 into the surrounding C- and E-row columns appeared roughly symmetrical. However, after DE-pairing between p7 and p17, the projection appeared to be more extensive over E- than C-row territories.

We used a polar analysis grid (termed from here on an analysis "pinwheel") for quantitative analysis of the axonal projections from the injections site into surrounding areas. The pinwheel was made up of numerous individual elements (see Methods for element characteristics), with the total length of all axons in each element being returned by the analysis tool used (see P. J. Broser et al., submitted for publication; and Methods). The radius of the pinwheel used for analysis of layer 2/3 sections was 750 μm, with a circular area around the center of the injection site with a radius of 250 μm excluded due to the high density of labeled structures. The location and size of the pinwheels used to analyze the 2 example

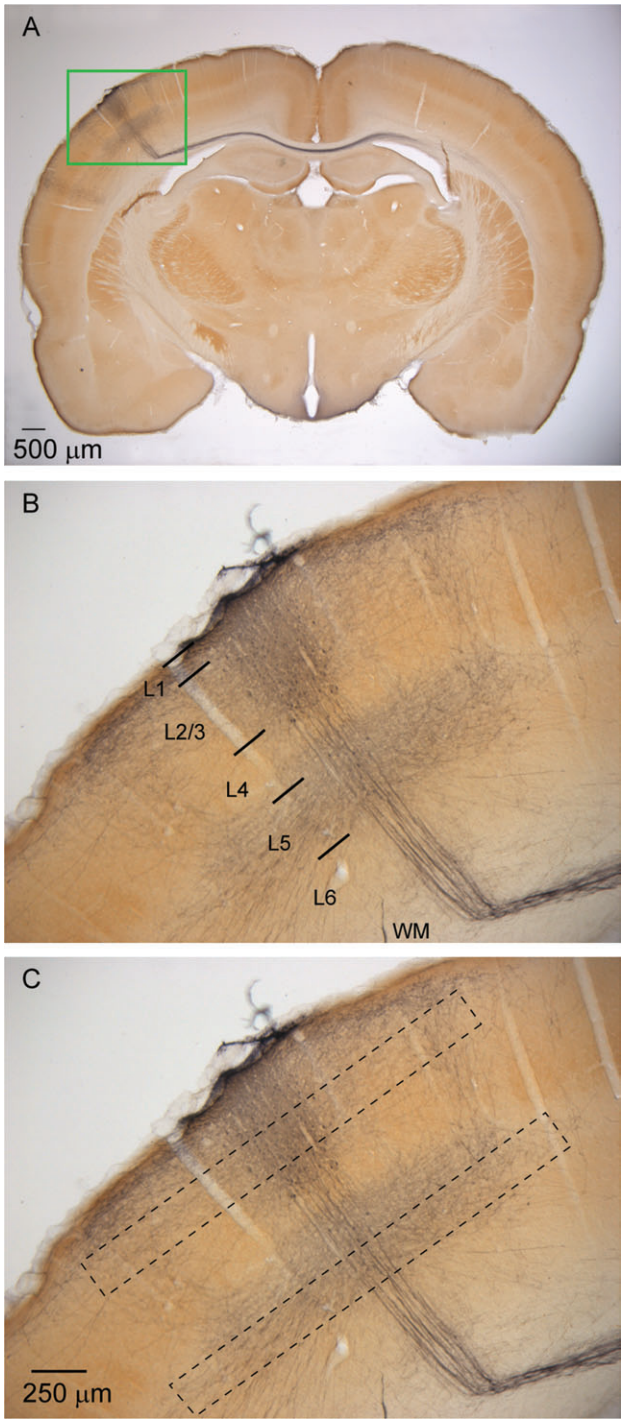

Figure 1. Axonal projection pattern from labeled layer 2/3 pyramidal neurons in coronal section. (*A*) Coronal section showing the axonal projections from a population of layer 2/3 neurons in the D2 column labeled via lentiviral mediated expression of GFP. Note the prominent projection from these cells to the contralateral hemisphere. The green rectangle outlines the area shown enlarged in panels (*B*) and (*C*). (*B*) Enlarged view of the region outlined by the green rectangle in panel (*A*). Note prominent horizontal projections in layer 2/3 and also in the infragranular layers giving the characteristic "hourglass" or "butterfly" appearance. Note also the axons projecting radially down the column through layer 4 and the infragranular layers and then turning in the white matter toward the corpus callosum. Approximate layer boundaries are indicated. WM, white matter. (*C*) Micrograph as is (*B*), but showing approximate depths and horizontal range in which, in tangential sections, axonal lengths were quantified (dashed black rectangles). Scale bar in (*C*) also applies to (*B*).

experiments in Figure 2 are shown in red in Figure 2*A2* and *B2*, with the zero degree axis of the pinwheel represented by the green line (see Methods for full details of orientation and placement of pinwheels). Axonal density maps for these 2 example experiments are shown in Figure 3. Comparison of these density maps suggests that the control animal the projections toward the C- and E-row columns are approximately symmetrical, whereas the DE-paired animal the projection is denser over E-row columns.

The fact that the absolute number of neurons labeled varied considerably between experiments required that analyses used either a ratiometric approach or used data normalized to a suitable reference. To test for gross changes in the projection patterns we first used a ratiometric approach. As an initial comparison we simply divided the pinwheel into a C-row facing and E-row facing half and compared C- to E-row ratio values between the control and paired groups (Fig. 4*A*). The average C- to E-row ratio for the paired group was lower than that for control, though this difference was not statistically significant (control C- to E-row ratio mean 1.049 ± 0.12, median 1.031, $n = 8$, DE-paired mean 0.930 ± 0.11, median 0.875, $n = 7$, $P = 0.12$). We next tested for more regionally selective alterations in the axonal projection pattern by defining 4 regions of interest (quadrants) and calculating the 4 possible C- to E-row ratios (Q1/Q3, Q1/Q4, Q2/Q3, and Q2/Q4, see Methods for further details). The locations of the 4 quadrants as well as their locations relative to an average barrel pattern, and the distributions of the calculated ratios are shown in Figure 4*B*. In all cases, the median ratio for the DE-paired group was less than that for the control group. Quadrant 1/3 and 2/3 ratio comparisons were considered significantly different after correction for multiple comparisons (Quadrant 1/3, control mean 1.13 ± 0.06, median 1.08, $n = 8$, paired mean 0.89 ± 0.05, median 0.90, $n = 7$, $P = 0.02$; Quadrant 2/3, control mean 1.15 ± 0.08, median 1.08, $n = 8$, paired mean 0.93 ± 0.03, median 0.93, $n = 7$, $P = 0.02$; note that these comparisons would not be considered statistically significant using the Bonferroni correction for multiple comparisons).

As the above ratiometric approach suggested that the changes were regionally specific, being significant for comparisons of both C-row quadrants against Quadrant 3 on the E-row side but not Quadrant 4, we next used a normalization approach to begin to analyze the nature of the changes in each quadrant in more detail. This approach involved normalizing the axonal length measured in the region of interest by the total axonal length measured in the whole analysis pinwheel (i.e., 0–360°) in all supragranular and infragranular sections. In effect, the values generated by this analysis represent the fraction of the total length of all axons detected that resides in the segment being analyzed, thus these normalized values are referred to form here on as quadrant fractional lengths. Results of this analysis are shown in Figure 5. Quadrant fractional length values for quadrant 3 were if anything slightly smaller for the DE-paired than for control group (control mean 0.087 ± 0.009, median 0.084, $n = 8$, paired mean 0.082 ± 0.004, median 0.086, $n = 7$, $P = 0.98$), suggesting that the reduction in quadrant ratios described above did not result from an increased axonal projection in this quadrant. Consistent with this, quadrant fractional lengths calculated for Quadrants 1 (control mean 0.077 ± 0.006, median 0.072, $n = 8$, paired mean 0.059 ± 0.003, median 0.062, $n = 7$, $P = 0.03$) and 2 (control mean 0.078 ± 0.007, median 0.079, $n = 8$, paired

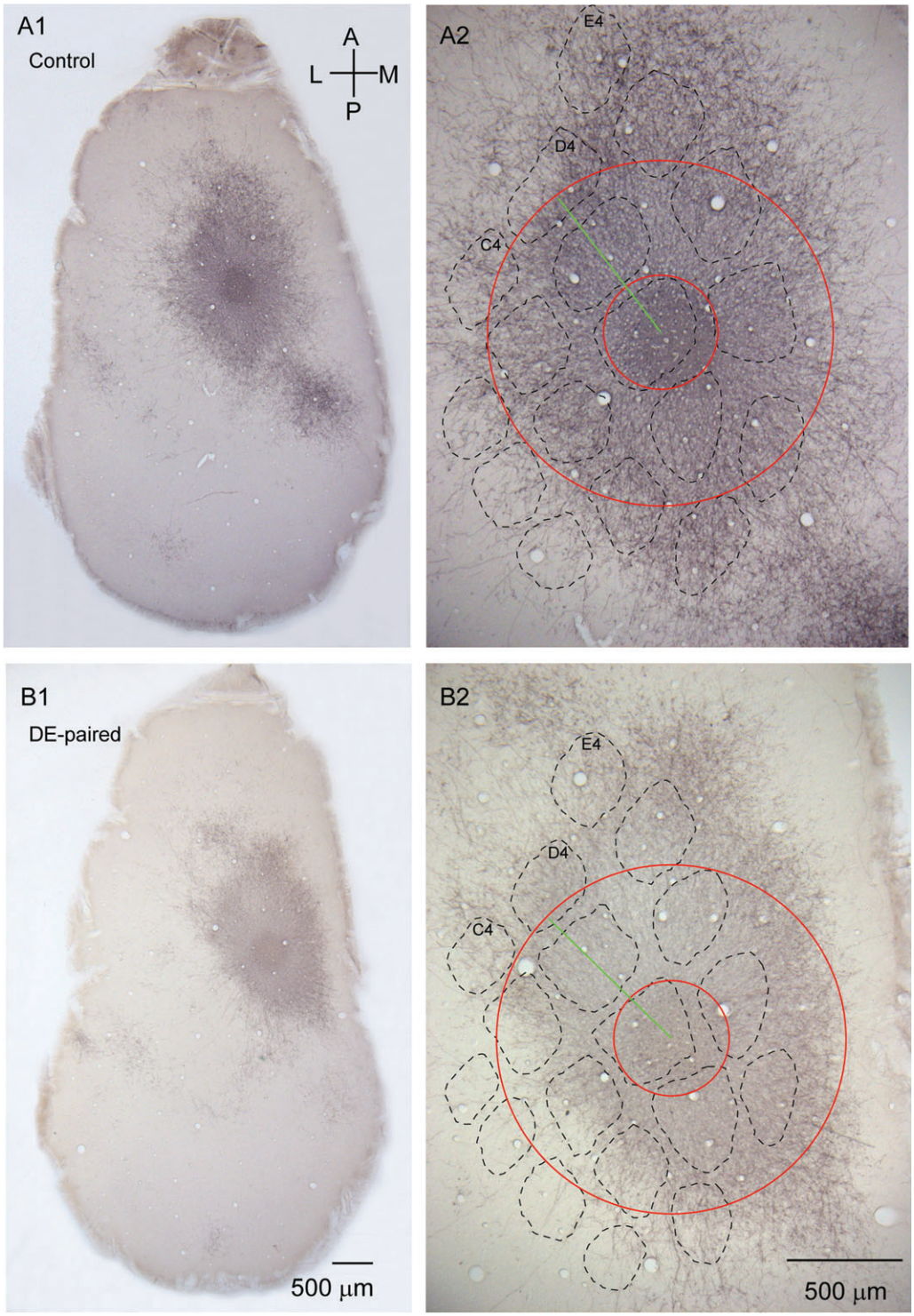

Figure 2. Horizontal projections in layer 2/3 from labeled layer 2/3 pyramidal neurons. (*A1*) Micrograph showing the layer 2/3 axonal projection pattern from the GFP-labeled layer 2/3 pyramidal neurons in a tangential section from a control animal. The injection site is visible as the darker spot in the center of the labeled projection pattern. (*A2*) Enlargement of the axonal projection pattern shown in (*A1*), showing the position, size and orientation of the analysis pinwheel. The zero degree axis is marked by the green line, and the outer limit and inner exclusion zone around the injection center are marked by the red circles. (*B1*) Layer 2/3 axonal projection pattern in a DE-paired animal. The injection was into the D2 column, and the injection site is again visible as the dark spot in the center of the projection pattern. (*B2*) Enlargement of the projection pattern shown in (*B1*). Both control and DE-paired sections are from 450 to 500 μm below the pia. The barrel patterns shown were reconstructed for each animal from cytochrome oxidase-stained sections in layer 4. Scale bars in (*B1*) and (*B2*) apply also to (*A1*) and (*A2*) respectively. Orientation guide in (*A1*) applies to all panels.

mean 0.064 ± 0.004, median 0.068, $n = 7$, $P = 0.07$) were lower in the DE-paired group than in the control group, though neither difference was considered statistically significant. Also of note, quadrant fractional lengths calculated for quadrant 4 were also lower in the DE-paired than control group (control mean 0.080 ± 0.010, median 0.073, $n = 8$, paired mean 0.068 ± 0.004, median 0.070, $n = 7$, $P = 0.44$). We also performed this analysis for the C- and E-row segments (Fig. 5*B*). C-row

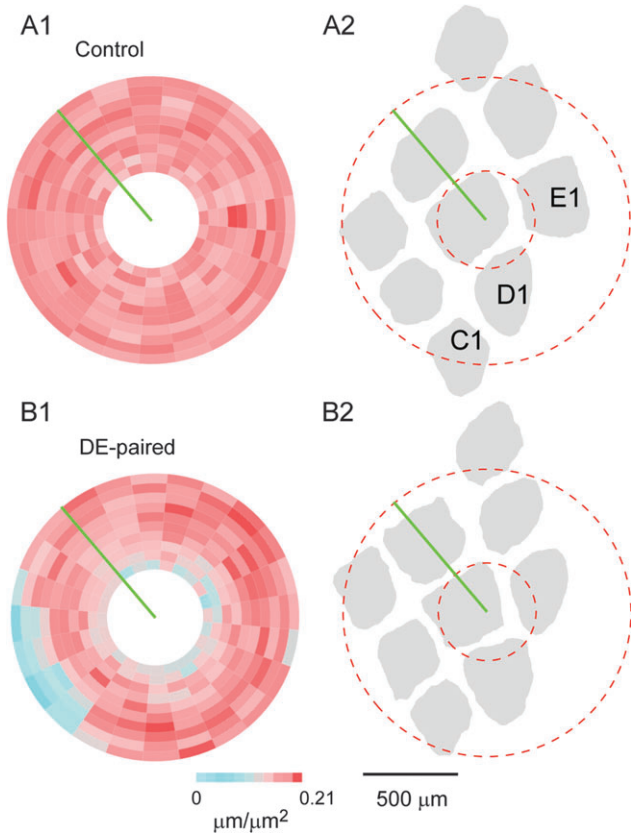

Figure 3. Axon density pinwheels. (*A1*) Axon density pinwheel for the control example shown in Figure 2*A*. (*A2*) Schematic diagram showing the positions of the C-, D- and E-row barrels relative to the analysis pinwheel (dashed red) and zero degree axis (green line) for the control example. The barrel pattern was reconstructed from cytochrome oxidase-stained layer 4 sections from the same control animal. (*B1*) Axon density pinwheel for the DE-paired example shown in Figure 2*B*. (*B2*) Barrel pattern schematic for the DE-paired animal. Note approximate symmetry of axonal densities on the C-row and E-row sides for the control pinwheel, and the asymmetry in the density in C- and E-row regions in the DE-paired example. Scale bars apply to all panels.

segment fractional lengths were significantly smaller for the DE-paired group (control mean 0.155 ± 0.013, median 0.147, $n = 8$, paired mean 0.123 ± 0.007, median 0.125, $n = 7$, $P = 0.04$), whereas values for the E-row segment were not different between the 2 groups.

Although the lentiviral injections were all located above the D2 barrel in layer 4, the exact location of the center of the injection relative to the borders of the barrel varied between animals. To test whether the site of the injection within the barrel influenced the measured asymmetry of the axonal projection, we first made a plot of the approximate position of the center of the injection site in layer 2/3 in relation to the layer 4 barrel pattern reconstructed from cytochrome oxidase–stained layer 4 sections. The locations of all control and DE-paired injection site centers relative to average barrel patterns for both groups are shown in Figure 6*A*. As the 2 groups appeared to have differing spatial distributions in the C-to-E axis, we designed a method to quantitatively compare the 2 distributions. The D2 barrel itself was in several cases difficult to precisely reconstruct as a consequence of the dense descending axonal projection from the labeled neurons (for example see Fig. S1*A*). We therefore defined a "C-row axis" (a straight line connecting the centers of the C2 and C3 barrels) and used this as the origin for comparison of the location of the injection site centers in the C-to-E axis (see Methods for further details). We also compared the distribution of the injection site centers in the D1-to-D3 axis (referred to as D-row spread). Scatter plots of the distributions of injection site locations in the C-to-E and D1-to-D3 axes are shown in Figure 6*B1* and *B2*, respectively. Although the spread in the C-to-E axis was greater for the DE-paired than for the control group and the mean also closer to the E-row side, there was no statistically significant difference between the distributions for the 2 groups (distance to C-row line control mean 426 ± 26 μm, median 403 μm, $n = 8$, paired mean 487 ± 37 μm, median 482 μm, $n = 7$, $P = 0.23$). To further examine the effect of the location of the center of the injection site on the symmetry of the axonal projection, we plotted the distance to the C-row axis against the quadrant ratios (Fig. 6*C*). There was no obvious relation between injection site location and any of the quadrant ratios for either the control or DE-paired group. Furthermore, when the relation between distance to the C-row line and the quadrant ratios was assessed using linear regression analyses no significant correlations were found (regression statistics given in Supplementary Table S1). The same was also true for investigation of the relation between injection site location in the C-to-E axis and quadrant fractional length (Fig. S2 and Supplementary Table S2), and also for investigations of the relation between injection site location in the D1-to-D3 axis and either quadrant ratios (Fig. 6*D*) or quadrant fractional lengths (Fig. S2). These analyses clearly indicate that the differences in the symmetry of the axonal projection pattern observed were not due to systematic differences in injection site location.

In summary, the above results suggest that DE-pairing causes an alteration in the axonal projection pattern of layer 2/3 pyramidal neurons in supragranular regions in such a way that neighboring used cortical areas (i.e., areas with preserved sensory input) end up with a denser axonal projection than the neighboring deprived areas. Moreover, the fractional length analyses suggest that there is a generalized reduction in axonal projection density in the DE-paired animals, consistent with the effects of sensory deprivation on axonal projections observed in visual cortex (Antonini and Stryker 1996, 1998).

Axonal Projection Patterns in Infragranular Layers

Coronal sections showed that labeled layer 2/3 neurons had dense axonal projections in infragranular layers in addition to their projections in supragranular layers. We therefore also analyzed the effect of DE-pairing on the axonal projection pattern in infragranular layers.

Representative examples of axonal projection patterns from labeled layer 2/3 neurons in infragranular sections are shown in Figure 7. As observed already in the supragranular sections, dense projections were observed in infragranular sections spreading in all directions around the injected column. However, in contrast to supragranular layers, the projection pattern in infragranular layers was not obviously changed after DE-pairing. Neither the C to E-row ratio analysis nor the quadrant analysis revealed any significant differences between the 2 data sets (Fig. 8). These results suggest that the infragranular projection of the labeled layer 2/3 neurons was not altered and that the axonal arborizations of these cells can

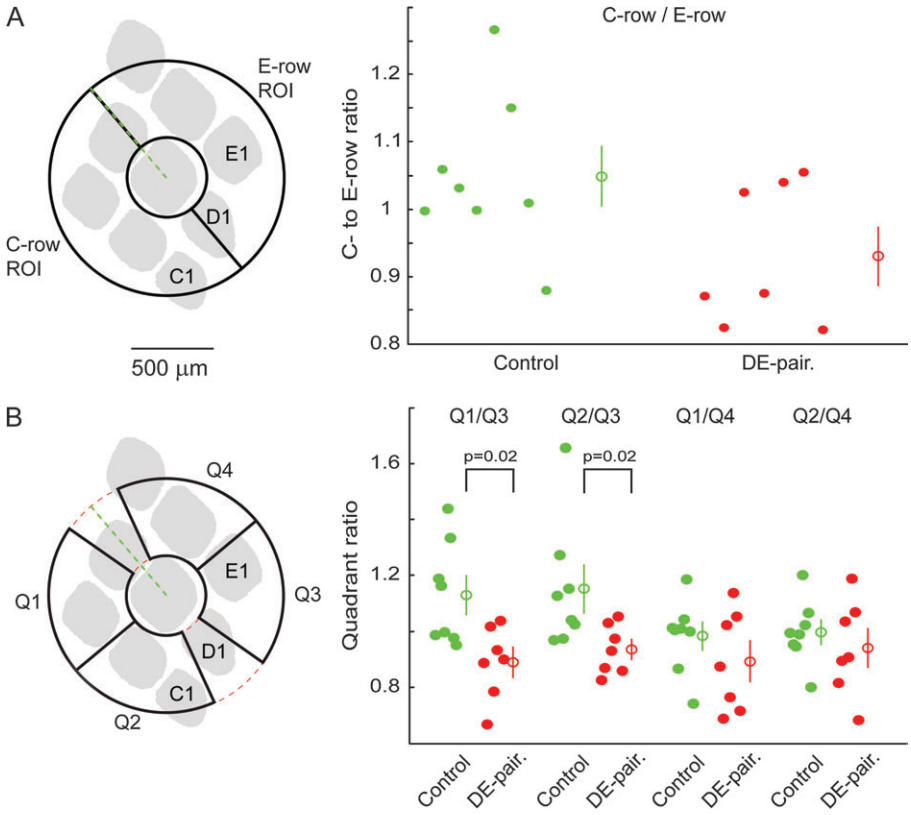

Figure 4. Ratio analysis of axonal projections in supragranular sections. (*A*) Scatter plot showing C- to E-row ratios for the control and DE-paired groups. Ratio values for the paired group tended to be lower than for the control group, though the difference was not statistically significant. (*B*) Scatter plots showing quadrant ratios for control and paired groups. Q1/Q3 and Q2/Q3 ratios were significantly smaller for the paired than for the control group. Distributions of Q1/Q4 and Q2/Q4 ratios were similar between the 2 groups. Open circles with error bars indicate mean ± standard error.

be modified by experience-dependent mechanisms in a layer-specific manner.

Altered Layer 2/3 Projection Pattern Results mainly from Reduced C-row Projection

The fractional length analysis of the supragranular data suggests that the differences in the ratios observed between control and DE-paired groups was due to a reduction in the projection of axons toward the deprived C-row columns rather than an increase in the projection to the E-row columns. A method used previously to analyze the extent and shape of the axonal projections from single filled cells has been to calculate 2-dimensional isolines to describe the projection domains (Brecht et al. 2003; Lübke et al. 2003). We used a similar approach to generate 3D contours with the intention of 1) further testing the possibility that the alterations in the axonal projection pattern in the supragranular region were due to a reduction in the projection toward the deprived C-row columns and 2) generating a more intuitive visualization of the spatial character of the normal axonal projection pattern and how this was altered by the DE-pairing. Average 60% 3D contours for the control and paired experimental groups are shown in Figure 9. These contours can be thought of as a 3D shape that contains 60% of the detected axons. The average 3D contours were calculated by determining a 60% 3D contour for each individual animal in each group and then calculating a normalized average 3D contour for each experimental group (see Methods for details). Figure 9*A* and *B* shows, from 2 different view angles, the average 3D contours for the 2 groups overlaid. The control contour is shown in semitransparent green and the DE-paired contour in solid red. In regions where the paired contour is smaller than the control one, the paired contour can be seen through the overlaid semitransparent control contour. Regions where the paired contour is larger appear solid red. In the supragranular region facing the C-row, the control contour was markedly larger than the paired contour (black arrow in Fig. 9*A*). The shape of the area in the supragranular layers where the control contour was larger (essentially the difference between control and paired contours) is shown in Figure 9*C*,*D*. The control contour was larger in almost all areas in the supragranular layers, consistent with a generalized reduction in the axonal arborization in the paired animals. In infragranular regions, both control and DE-paired contours were similar in size and shape, consistent with the results described above.

For quantitative comparison of the 2 sets of contours we calculated the volume of the contour within the row segments or the quadrants as a fraction of the total volume of the contour. Supragranular fractional contour volumes for the C- and E-row segments and for the quadrants are shown in Figure 9*E* and *F*, respectively. Fractional volumes for the C-row segments were significantly smaller for the DE-paired group than for the control group (C-row control mean fractional isosurface volume 0.171 ± 0.014, median 0.152, n = 8, paired mean 0.128 ± 0.005, median 0.128, n = 7, P = 0.002). Similarly, fractional volumes were also significantly smaller for both the

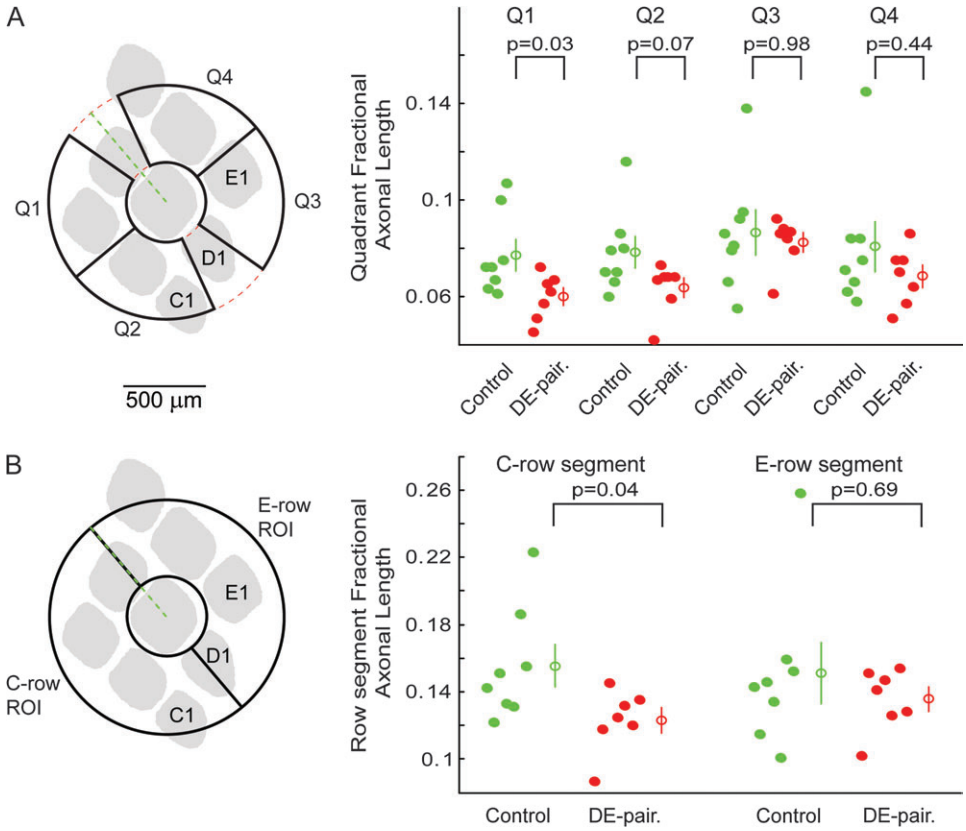

Figure 5. Fractional length analyses for supragranular layers. (*A*) Scatter plots of quadrant fractional length for each of the 4 quadrants for both control and paired groups. For all quadrants there was a tendency for fractional lengths to be lower for the paired group, though the differences were not considered statistically significant. (*B*) Fractional length analysis for C- and E-row segments. C-row segment fractional lengths for paired animals were significantly lower than for control counterparts. E-row fractional lengths were not different between the groups. The schematic diagrams in (*A*) and (*B*) show the approximate size and orientation of the quadrants and row segments respectively relative to an average barrel pattern. Open circles with error bars indicate mean ± standard error.

C-row facing quadrants (Quadrant 1 control mean fractional isosurface volume 0.070 ± 0.006, median 0.062, n = 8, paired mean 0.050 ± 0.003, median 0.051, n = 7, P = 0.002; Quadrant 2 control mean 0.070 ± 0.006, median 0.063, n = 8, paired 0.053 ± 0.003, median 0.055, n = 7, P = 0.006; both analyses considered significant after correction for multiple comparisons). Fractional volumes for both the E-row segment and E-facing quadrants were also smaller for the DE-paired group, though the differences were not statistically significant.

In summary, the 3D contour analysis indicates that there is a generalized reduction in the size of the contour in supragranular regions in the DE-paired group, with a particularly prominent and statistically significant reduction in the contour facing the C-row columns. Taken together with the results of the ratio and fractional length analyses, the results suggest that the DE-paired group has a generalized reduction in the total length, density, or complexity of the axonal projection in the supragranular regions with a particularly prominent and highly significant reduction in the projection toward the deprived C-row columns.

Discussion

We show that axonal arbors of layer 2/3 pyramidal neurons in rat barrel cortex can be altered by a period of whisker trimming. A cortical deprivation pattern that surrounds a cortical column with used areas on one side, and deprived areas on the other, results in a reduced total axonal load projecting toward the deprived columns. This reduced projection could result from either a retraction of axons that had already grown into the deprived region or alternatively, from a failure of axons to grow or be stabilized in the deprived area. The results are consistent with data from a recent study which show, using vsd-imaging, that this deprivation paradigm results in reduced spread of the vsd signal toward the deprived columns (Wallace and Sakmann 2007). These anatomical findings thus provide a plausible anatomical explanation for the functional changes observed.

Effects of Trimming during the Critical Period for Layer 2/3

The main effect of the sensory deprivation was a reduction in the total load of axons projecting into the deprived cortical area. The volume of the 3D-projection domain facing the deprived cortical territories reduced in DE-paired animals by about 18%. Extracting from this the effect on the axonal arborization of individual cells is complicated by the fact that the viral injections labeled variable numbers of cells, and obtaining accurate estimates of the number of cells labeled in each individual experiment was not possible. The density of the stained structures in the area directly surrounding the injection site made assessment of whether an individual cell soma was stained or not a rather variable decision. Rough estimates of the number of labeled cells made by estimating the number of

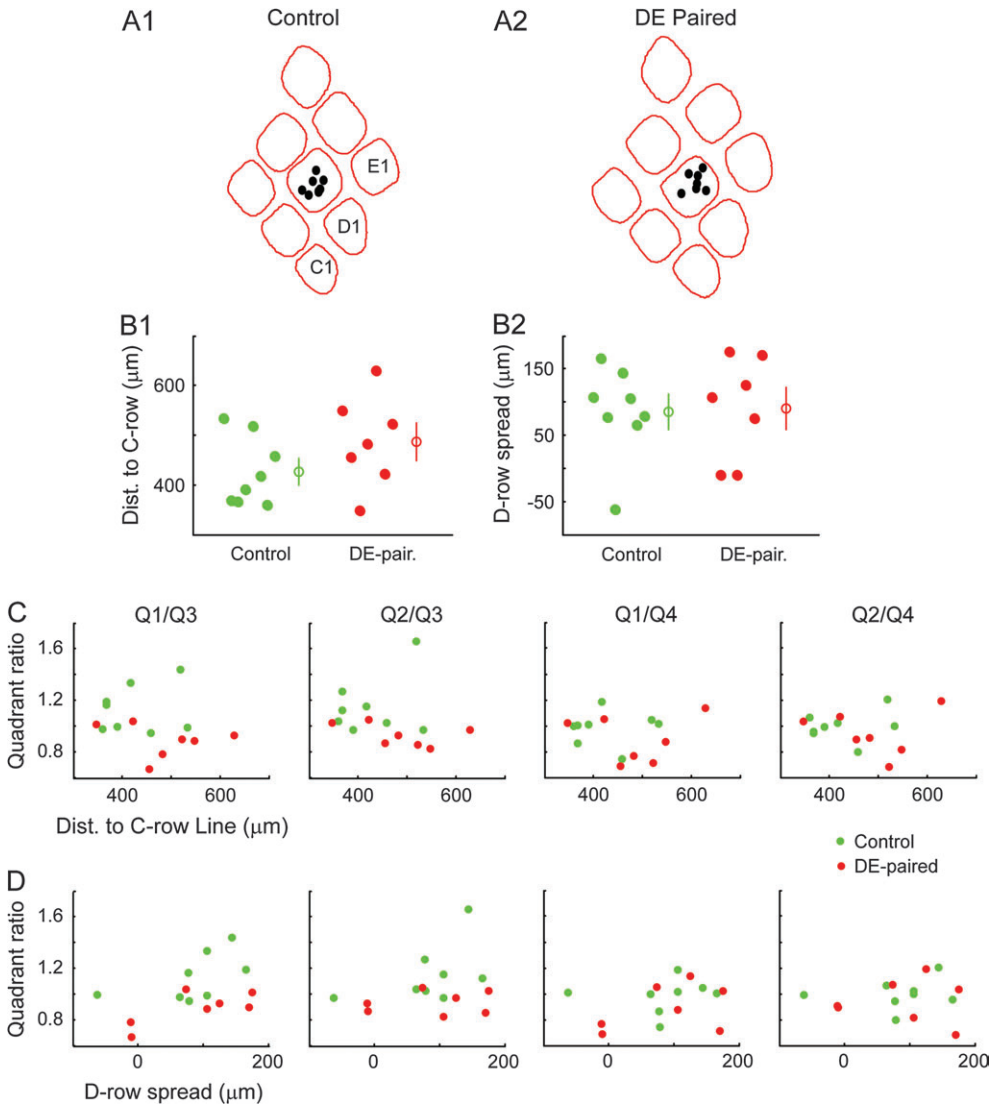

Figure 6. Measures of the axonal projection asymmetry are not influenced by variations in the location of the injection site within the D2 column. (*A1* and *A2*) Locations of the injection site centers in layer 2/3, for control, (*A1*), and DE-paired, (*A2*) groups, superimposed on average barrel patterns. The average barrel patterns were calculated from individual reconstructions of the layer 4 barrel pattern for each animal in each group. (*B1* and *B2*) Scatter plots showing the distribution of distances from the injection site center to the C-row line, (*B1*), and D-row spread of the injection site centers, (*B2*), for the control and paired groups. The C-row line was defined, for each animal, as a line connecting the centers of the C2 and C3 barrels. The distance from injection site center to the C-row line was designed to provide a measure of the location of the injection site along the arc-axis of the D2 column (see Methods for details). Similarly, the D-row spread measure was designed to provide a measure of the injection site location along the row-axis of the D2 column. The spread of the injection site locations along the arc-axis was greater for the paired group and the mean distance to the C-row line slightly larger (slightly closer to the E-row columns). However, the distributions of distances to the C-row line were not statistically different between the 2 groups. Distributions of injection site locations along the row-axis were also not different between the groups. Open circles with error bars indicate mean ± standard error. (*C*) Plots of quadrant ratios against injection site location in the arc-axis (distance to C-row line). There was no obvious correlation between the 2 variables for any of the quadrant ratios for either control or DE-paired group, indicating that the location of the center of the injection site along the arc-axis does not influence the measured asymmetry of the axonal projection. (*D*) Plots of quadrant ratios against injection site location in the row-axis. As for the analysis of the influence of injection site location in the arc-axis, the location of the injection in the row-axis also had no effect on the measured asymmetry of the axonal projection.

stained axons and axon bundles which were passing radially down the column through the infragranular sections yield an estimated reduction in the length of the supragranular axonal arbor of about 650 μm per cell. This estimate should be interpreted cautiously because of the uncertainty in estimation of the number of labeled neurons. However, it provides an order of magnitude indication of the differences in axonal arbor lengths between the 2 experimental groups.

It is at this stage unclear why the ratiometric analysis of the data from the supragranular region found significant differences between control and DE-paired animals for the Q1/Q3 and Q2/Q3 ratios, but not for Q1/Q4, Q2/Q4, or C- versus E-row ratios. The fractional length analyses (Fig. 5) suggest that, numerically at least, the primary reason for this was that although Q1, Q2, and Q4 all have lower fractional lengths in DE-paired than in control animals, the difference for Q3 is considerably less. One possible explanation lies in the substantial projection from barrel cortex to a cortical area just posterior and medial to the barrel cortex. This projection, which may target the area referred to as the parietal association cortex (Paxinos and Watson 1998), generally ran posterior medially from the injected D2 column, meaning that some of

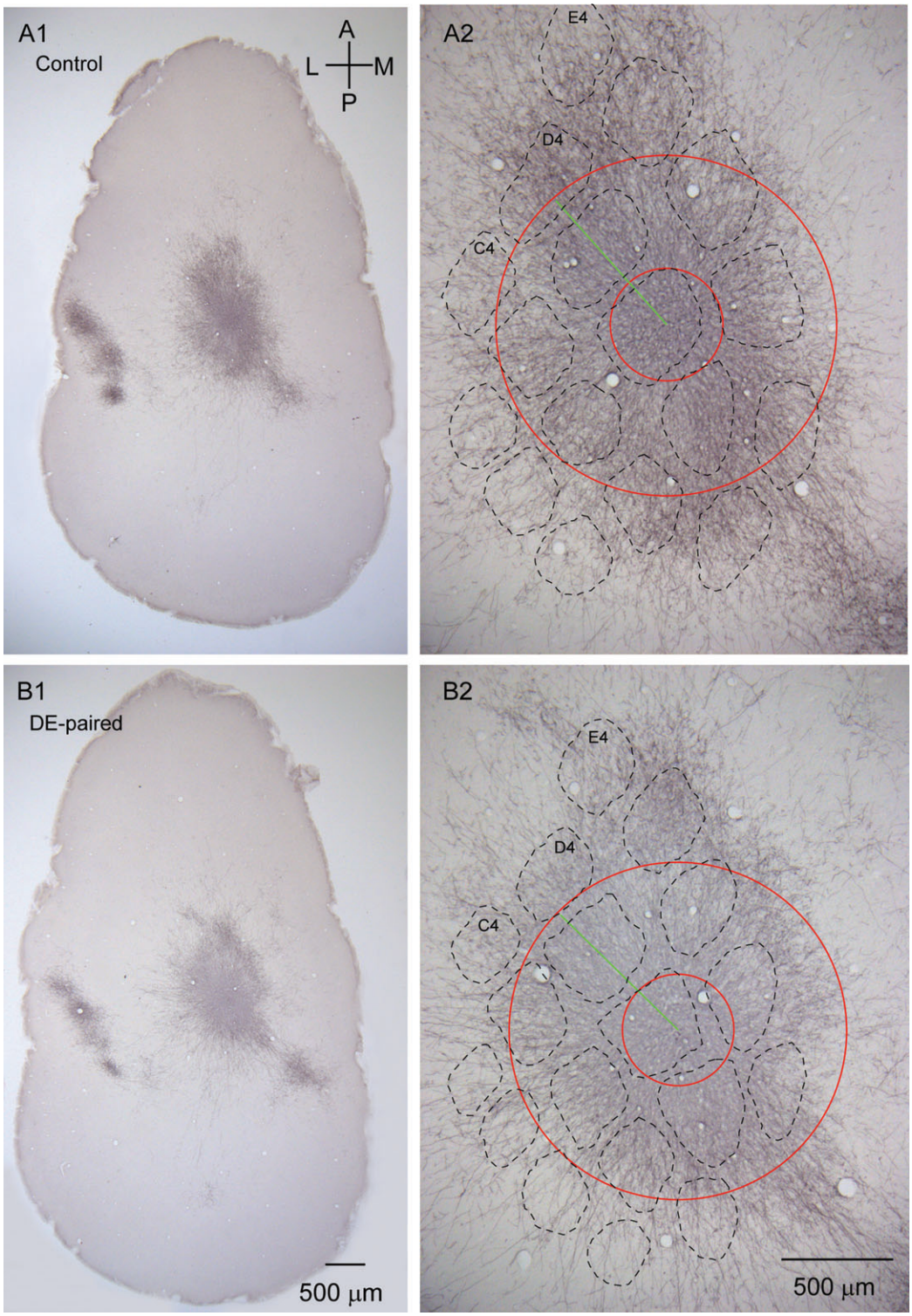

Figure 7. Axonal projection pattern from labeled layer 2/3 neurons in infragranular layers. (*A1*) Micrograph showing the axonal projection pattern of the labeled population of layer 2/3 pyramidal neurons in an infragranular section (1000–1050 μm below the pia) in a control animal. (*A2*) Enlargement of the axonal projection around the injection site in the micrograph shown in (*A1*) with an overlay of the size and orientation of the analysis pinwheel. Conventions regarding pinwheel as for Figure 2. (*B1*) Micrograph of the axonal projection pattern in a DE-paired animal. The section was 1050–1100 μm below the pia. (*B2*) Enlargement of the injection site shown in the micrograph in (*B1*). Sections are from the same control and DE-paired animal as those shown in Figure 3. Barrel patterns shown are reconstructed from cytochrome oxidase-stained layer 4 sections. Scale bars in (*B1*) and (*B2*) apply also to (*A1*) and (*A2*), respectively. Orientation guide in (*A1*) applies to all panels.

this projection may be captured in the Q3 quadrant. Assuming this projection was not substantially changed by the deprivation paradigm, it is conceivable that its presence may lead to higher fractional lengths in Q3 than in Q1, Q2, or Q4 in the DE-paired animals. However, this is pure speculation, and we currently have no clear explanation why in the DE-paired animals Q3 fractional lengths are less changed than Q1, Q2, and Q4.

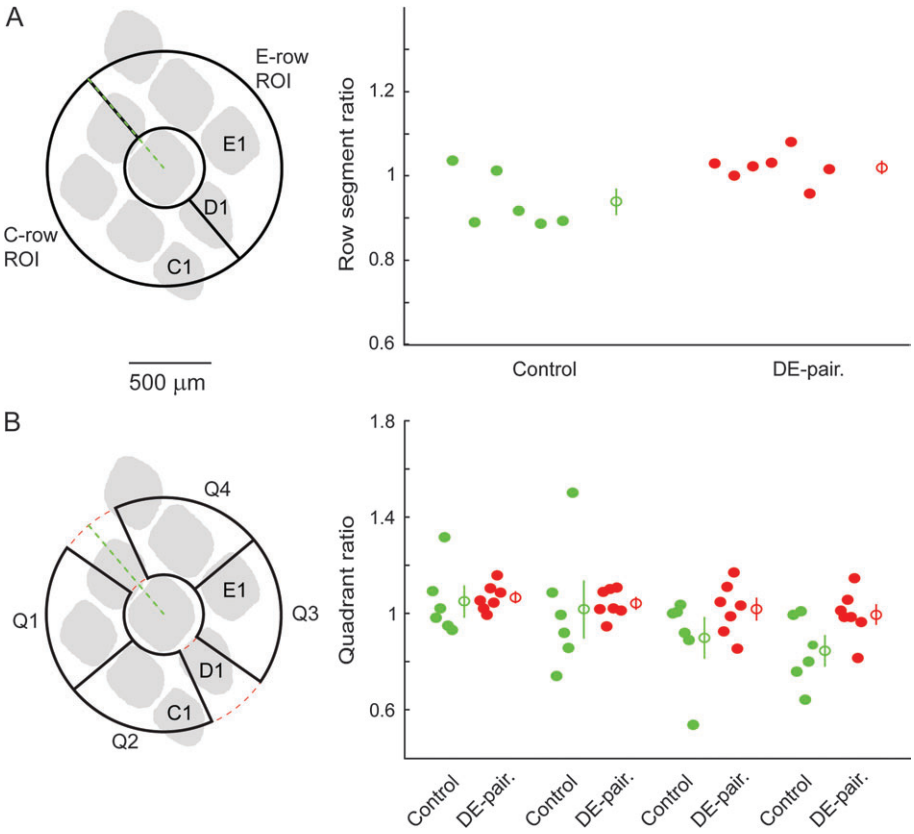

Figure 8. Axonal projection patterns from layer 2/3 neurons in infragranular layers are not modified by DE-pairing. (*A*) Scatter plot of the C- to E-row ratio analysis performed on data from infragranular sections. C- to E-row ratios were not different between the 2 experimental groups. (*B*) Scatter plots showing the quadrant ratio analysis for infragranular sections. Unlike the results from this analysis for the supragranular layers, none of the quadrant ratios were significantly different between the 2 groups. The size and approximate orientation of the C- and E-row regions of interest in which axonal lengths were quantified for calculation of the C- to E-row ratios are shown in the schematic diagram next to the plot in (*A*). Similarly, the analysis quadrants are shown in the schematic diagram next to the plot in (*B*). Open circles with error bars indicate mean ± standard error.

Correlation with Functional Results

The results of this anatomical study are consistent with the results presented in a companion report, which investigates functional consequences of the same whisker trimming protocol using vsd-imaging (Wallace and Sakmann 2007). The vsd study showed that DE-pairing during the second and third postnatal week resulted in the development of an asymmetry in the spread of the vsd signal around the cortical column representing the stimulated D-row whisker, favoring spread toward the neighboring nondeprived E-row cortical columns. The bias resulted primarily from a reduction in the spread of the vsd signal toward the deprived C-row columns. Interestingly, the vsd signal spread toward E-row columns was also slightly reduced in DE-paired animals, with the pronounced asymmetry resulting from the even stronger decrease in spread toward the C-row. In combination, these results support the interpretation that the primary effect of the DE-pairing protocol is to reduce the extent of the layer 2/3 projection from D-row columns toward the neighboring deprived columns. Functionally, this manifests itself as a reduction in the capacity of layer 2/3 to elicit subthreshold activity in the deprived cortical areas.

In the vsd study, it was also shown that symmetrical responses could be restored in previously DE-paired animals by allowing the whiskers to regrow for around 10 days. After regrowth of the whiskers, the observed responses were not different to those recorded from control animals (Wallace and Sakmann 2007). To what extent this results from a corrective rebalancing of axonal projection densities is at this stage unclear. Experiments in visual cortex examining morphological changes accompanying recovery from the effects of monocular deprivation induced by a reverse-suture paradigm reveal that axonal arbors from thalamic cells serving the formerly deprived eye show some corresponding increase in complexity and total length (Antonini et al. 1998). It may then be expected that upon regrowth of the whiskers in the DE-pairing model there is an accompanying increase in axonal projection density in the deprived cortical columns that matches the re-establishment of symmetrical functional responses. The other alternative, that the re-establishment of symmetrical responses occurs through modifications of the strengths of individual connections, although still conceivable, seems less likely.

It should be noted that the experiments described here employ a whisker trimming protocol that covers a critical period of the development of layer 2/3 of somatosensory cortex, and the effects observed may well be very different to those seen in adult animals. For example, one previous study has examined potential changes in axonal projection pattern in the barrel cortex of adult mice after a deprivation protocol that spared all whiskers in the C-row (Kossut 1998; Kossut and Juliano 1999). In these experiments, neurons in the column representing one of the spared whiskers were labeled by injections of fluororuby or fluoroemerald made into acute slices taken from deprived or nondeprived animals. The authors

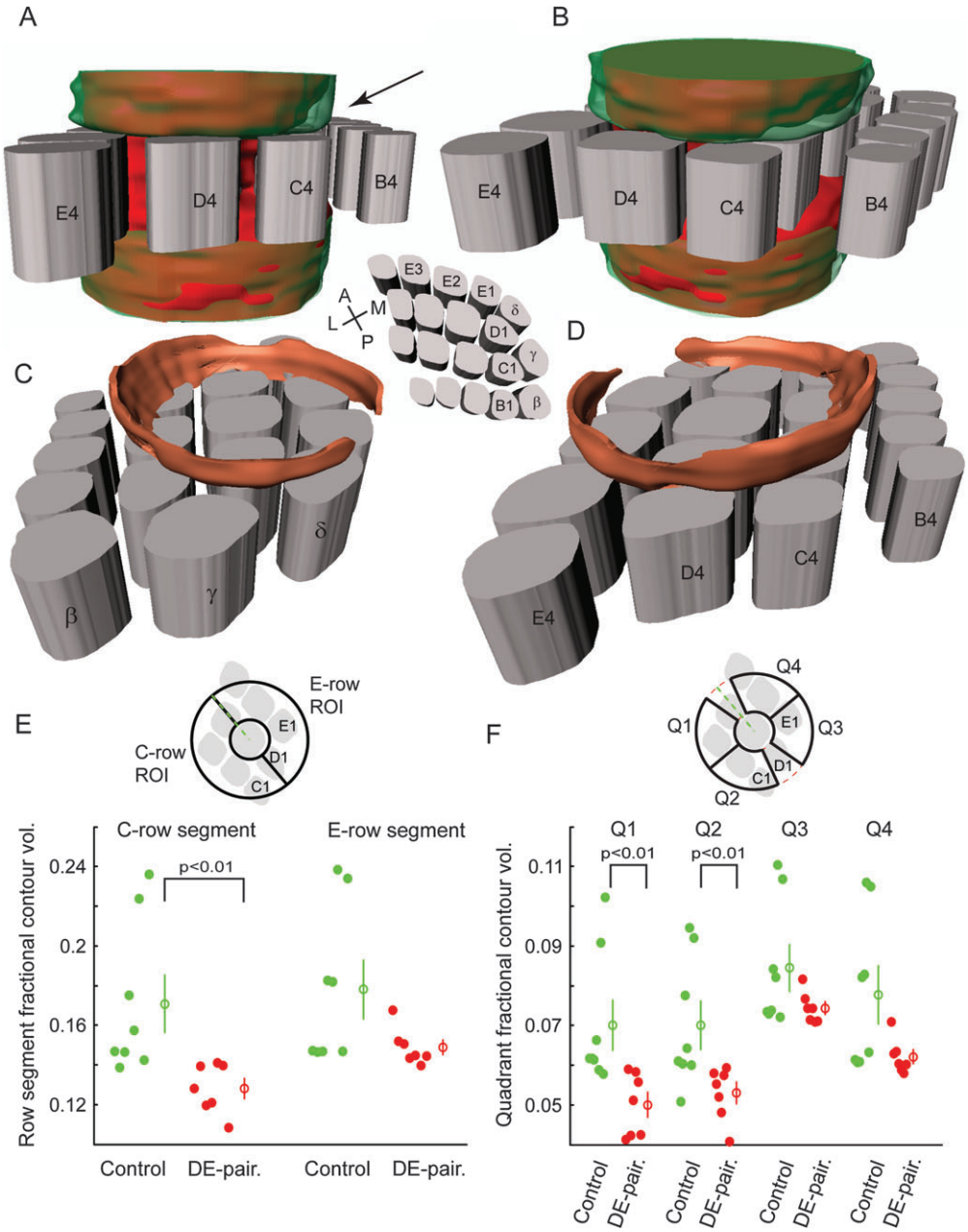

Figure 9. Analysis of 3D contours shows DE-pairing causes a reduction in axonal projections toward deprived columns. (*A* and *B*) Views from 2 different perspectives of the overlaid 3D contours for both the control (semitransparent green) and DE-paired (solid red) experimental groups. The shape of the paired contour can be seen through the control contour in areas where the control contour is larger. Areas where the paired contour is larger appear as solid red. Note that in the supragranular layers the paired contour is generally smaller than the control contour, and that this difference is particularly marked over the C-row columns (black arrow in *A*). (*C* and *D*) Illustrations showing the areas in the supragranular layers where the control contour is larger than the DE-paired one (essentially the difference between the control and paired contours). The control contour was larger in most regions of the supragranular layers, with a marked difference present over the C-row columns. The average barrel pattern shown was calculated from all animals in the control group and is for illustrative purposes only. Scaling varies between images as a consequence of the 3-dimensional representations, but as an indication the barrels in all cases are 400 μm high. (*E*) Scatter plots showing C- and E-row segment fractional contour volumes (the volume of the contour within the segment as a fraction of the total contour volume). Fractional volumes for C-row segments in the paired group were significantly smaller than those for the control group. (*F*) Scatter plots of fractional contour volumes for the 4 analysis quadrants. Fractional quadrant volumes for quadrants 1 and 2, facing the C-row columns, were significantly smaller in the paired group. Quadrant fractional volumes for the E-row facing quadrants were also smaller in the paired group, consistent with a generalized reduction in axonal projections, though the differences for these quadrants were not statistically significant. Open circles with error bars indicate mean ± standard error.

found that axons measured from deprived animals were some 60–80% longer than those measured from control animals. Consistent with this, the results showed that the same whisker sparing protocol results functionally in an increase in the extent of the area of active cortex as measured by 2-deoxyglucose mapping. It is therefore possible that different mechanisms are operating during early postnatal development and in the adult cortex.

Possible Mechanisms

The pyramidal neurons in layer 2/3 of the barrel cortex are known to be developing extensively during the period of the

sensory deprivation in this study, both in terms of their cellular morphology and their synaptic connectivity. At p8, layer 2/3 pyramidal neurons in both rat (G. Radnikow and D. Feldmeyer, personal communication) and mouse (Larsen and Callaway 2006) have extensive projections within the surrounding layer 2/3 area. Under normal conditions, both the total length and the complexity of these projections increase substantially between p8 and p21 (Larsen and Callaway 2006). It is most likely therefore that the results of the current study indicate an alteration in the normal development of these axonal projections from the layer 2/3 pyramidal neurons in the D2 column. The alteration may take the form of either a loss of existing axon segments projecting toward the deprived C-row columns, a failure of new axon segments to develop or a combination of both.

One possible mechanism is that under normal conditions, activity of C-row columns results in release of a growth factor or other neurotrophic agent, and that the axonal processes of the D-row layer 2/3 neurons extend toward C-row along the gradient of this factor or are stabilized by its presence. The presence or absence of activity in the C-row columns would be sufficient to modify axonal projections under this scheme.

An alternative mechanism is based on the growing body of evidence suggesting that axon extensions occur at stabilized synapses (Alsina et al. 2001; Cohen-Cory 2002; Hu et al. 2005; Meyer and Smith 2006; Ruthazer et al. 2006), in combination with a variation on "neurotrophic hypothesis" advanced initially to describe formation of ocular dominance columns (Katz 1999; Kandel et al. 2000). According to this hypothesis, activity in the postsynaptic neuron causes the release of a neurotrophic (or other) factor from the postsynaptic side of the synapse. When the activity of the presynaptic neuron is correlated with that of the postsynaptic neuron, the neurotrophic factor is endocytosed by the presynaptic bouton (for example during vesicle reuptake). Availability of the factor to the presynaptic bouton then stabilizes or maintains the synapse. In contrast, if the activity of the pre- and postsynaptic neurons is not correlated, then the factor is not taken up and therefore not available to the presynaptic bouton and the synapse as a consequence atrophies. As far as the current results are concerned, the suggestion would be that in untrimmed animals, correlated activity between the presynaptic neuron in the D-row column and postsynaptic neuron in the C-row column would lead to stabilization of synapses in the connection between D-row and C-row cells, and hence continued branching and extension of axon from D-row cells toward the neighboring C-row columns. In contrast, after trimming of C-row whiskers, and therefore presumably a considerable reduction in correlated activity between neurons in layer 2/3 of C- and D-row columns, fewer synapses would be stabilized, and thus the axonal processes from the D-row neurons would be reduced in length or number of branches or both.

Layer Specificity of Axonal Arbor Modifications

Characteristically, individual pyramidal neurons in layer 2/3 of barrel cortex have dense axonal arborizations in both layer 2/3 and in layer 5 (Gottlieb and Keller 1997; Feldmeyer et al. 2006; Larsen and Callaway 2006). Consistent with this, the labeled populations of layer 2/3 neurons studied here had extensive projections to infragranular layers. Surprisingly, these layer 5 projections were not significantly affected by DE-pairing, even though a pronounced effect was observed on the arborization of the same cells in layer 2/3. One possibility is that the layer 5 arborizations are altered in a more subtle manner and that we are unable to detect the effects using bulk labeling techniques. Given that we exclude the area close to the injection site from our analyses, we can also not exclude the possibility that changes of the layer 5 axonal arbors are within this area.

Studies comparing usage-dependent plasticity across the different cortical laminae in the visual cortex of several species (Hubel et al. 1977; Shatz and Stryker 1978; Gordon and Stryker 1996; Issa et al. 1999; Trachtenberg et al. 2000) have found that changes can be detected in layer 5 at the same time as those observed in layer 2/3 and that the magnitude of the alterations is similar in the 2 layers. The functional consequences of the DE-pairing protocol used here have not yet been established for the infragranular layers, and it is conceivable that longer periods of sensory deprivation are required for alterations of the layer 2/3 arbors in infragranular layers. However, Diamond et al. (1994) found that a whisker trimming protocol similar to that employed here resulted in significant functional changes in infragranular neurons in adult rats only 24 h after whisker trimming. With this precedent in mind it is reasonable to assume that the trimming protocol used here would also result in functional changes in infragranular layers. If this was the case, the current work would suggest that the anatomical substrate is not the axonal arbors of the overlying layer 2/3 neurons. However, it is important to note that the functional effects of the DE-pairing protocol have been shown to have a critical period ending around the end of the second postnatal week, and the current work has employed a trimming protocol within this critical period. This plasticity could thus be different to the form of plasticity expressed by the adult rats in the study by Diamond et al.

The anatomical finding presented here suggests that the long range projections from these layer 2/3 neurons can be modified in isolation, implying that the mechanisms that result in the observed changes act relatively locally. If there is a spike timing-dependent mechanism driving these changes it is perhaps not surprising that the effects are rather local given that they would be centered about contacts between the individual cells. Finally, layer 5 neurons also project to several subcortical structures in addition to their cortical projections, whereas layer 2/3 neurons project to cortical areas (Nauta and Bucher 1954; Wise and Jones 1977b, 1977a; Peters and Jones 1984). The differences in anatomical malleability may therefore reflect these differences in projection targets. That is, perhaps experience-dependent modifications to the cortical circuit architecture may provide a benefit for cortical signaling efficiency, but not be of benefit to the cortical output to subcortical nuclei.

Similarities with Critical Period Deprivation Effects in Visual Cortex

In terms of the general phenomenology of reduced complexity and length of axonal arbors of neurons after sensory deprivation, the results of the current study are in some regards comparable with those reported for the developing visual system. In both the cat (Antonini and Stryker 1993, 1996) and the mouse (Antonini et al. 1999), monocular deprivation results in reduced cortical responsiveness to the deprived eye that is accompanied by a reduction in the total length and complexity of the geniculocortical axonal arbors serving that eye. Although anatomically these studies examine thalamocortical projections, while the current study uses a cortico-cortical projection as a model, it is not unreasonable to think that similar mechanisms may operate in both cases.

Within the visual system too, there is anatomical evidence to suggest that brief periods of disruption to normal visual input during development in such a way as to reduce the amount of correlated activity between 2 separated layer 2/3 regions also lead to reductions in axonal arbors projecting to regions with noncorrelated activity (Trachtenberg and Stryker 2001). In this study, the authors examined the distributions both of retrogradely labeled cells and of anterogradely labeled synaptic boutons following injections of tracers into subregions of cat area 17 functionally identified to be strongly dominated by one or other eye. These distributions were then compared between normally sighted kittens and kittens in which the optical axis had been misaligned surgically for brief periods around the time of the critical period for development for orientation preference in cat visual cortex. In control animals, the distributions of neurons and boutons labeled have a small bias toward other areas preferentially responding to the same eye. This bias is significantly increased after misalignment of the optical axis in a way consistent with a redistribution of the layer 2/3 axons away from areas not sharing correlated input. This result is comparable with the results of the current study, and suggests that this mechanism may be a general organizing principle for layer 2/3 during development.

Conclusions

The results of the present experiments demonstrate an anatomical correlate of functional changes shown to occur in layer 2/3 after DE-row pairing during the second and third postnatal week. The changes we observed in axonal projections from layer 2/3 pyramids were restricted to supragranular regions, with no evidence found for changes in the infragranular projections from these cells. This result suggests that structural modifications at subsets of a neurons axonal arborization may be possible. Functionally, DE-row pairing results in reduced spread of the subthreshold vsd signal toward the deprived C-row columns. We show here that this correlates with a reduction in the axonal arborization of layer 2/3 pyramidal neurons projecting toward the deprived cortical area.

Supplementary Material

Supplementary material can be found at: http://www.cercor.oxfordjournals.org/.

Funding

This article was produced with funding from the Max Planck Society and the Alexander von Humboldt Foundation, a fellowship granted to Dr. Damian Wallace.

Notes

Conflict of Interest: None declared.

Address correspondence to Damian Wallace, PhD Department of Cell Physiology, Max Planck Institute for Medical Research, Jahnstrasse 29, D-69120 Heidelberg, Germany. Email: dhw@mpimf-heidelberg.mpg.de.

References

Alsina B, Vu T, Cohen-Cory S. 2001. Visualizing synapse formation in arborizing optic axons in vivo: dynamics and modulation by BDNF. Nat Neurosci. 4:1093–1101.

Antonini A, Fagiolini M, Stryker MP. 1999. Anatomical correlates of functional plasticity in mouse visual cortex. J Neurosci. 19:4388–4406.

Antonini A, Gillespie DC, Crair MC, Stryker MP. 1998. Morphology of single geniculocortical afferents and functional recovery of the visual cortex after reverse monocular deprivation in the kitten. J Neurosci. 18:9896–9909.

Antonini A, Stryker MP. 1993. Rapid remodeling of axonal arbors in the visual cortex. Science. 260:1819–1821.

Antonini A, Stryker MP. 1996. Plasticity of geniculocortical afferents following brief or prolonged monocular occlusion in the cat. J Comp Neurol. 369:64–82.

Antonini A, Stryker MP. 1998. Effect of sensory disuse on geniculate afferents to cat visual cortex. Vis Neurosci. 15:401–409.

Armstrong-James M, Fox K, Das-Gupta A. 1992. Flow of excitation within rat barrel cortex on striking a single vibrissa. J Neurophysiol. 68:1345–1358.

Benjamini Y, Hochberg Y. 1995. Controlling the false discovery rate—a Practical and powerful approach to multiple testing. J Roy Stat Soc B. 57:289–300.

Brecht M, Roth A, Sakmann B. 2003. Dynamic receptive fields of reconstructed pyramidal cells in layers 3 and 2 of rat somatosensory barrel cortex. J Physiol. 553:243–265.

Bureau I, Shepherd GM, Svoboda K. 2004. Precise development of functional and anatomical columns in the neocortex. Neuron. 42:789–801.

Callaway EM, Katz LC. 1990. Emergence and refinement of clustered horizontal connections in cat striate cortex. J Neurosci. 10:1134–1153.

Callaway EM, Katz LC. 1991. Effects of binocular deprivation on the development of clustered horizontal connections in cat striate cortex. Proc Natl Acad Sci USA. 88:745–749.

Chapman B, Stryker MP. 1993. Development of orientation selectivity in ferret visual cortex and effects of deprivation. J Neurosci. 13:5251–5262.

Chapman B, Stryker MP, Bonhoeffer T. 1996. Development of orientation preference maps in ferret primary visual cortex. J Neurosci. 16:6443–6453.

Cohen-Cory S. 2002. The developing synapse: construction and modulation of synaptic structures and circuits. Science. 298:770–776.

Diamond ME, Huang W, Ebner FF. 1994. Laminar comparison of somatosensory cortical plasticity. Science. 265:1885–1888.

Dittgen T, Nimmerjahn A, Komai S, Licznerski P, Waters J, Margrie TW, Helmchen F, Denk W, Brecht M, Osten P. 2004. Lentivirus-based genetic manipulations of cortical neurons and their optical and electrophysiological monitoring in vivo. Proc Natl Acad Sci USA. 101:18206–18211.

Durack JC, Katz LC. 1996. Development of horizontal projections in layer 2/3 of ferret visual cortex. Cereb Cortex. 6:178–183.

Feldman DE, Brecht M. 2005. Map plasticity in somatosensory cortex. Science. 310:810–815.

Feldmeyer D, Lübke J, Sakmann B. 2006. Efficacy and connectivity of intracolumnar pairs of layer 2/3 pyramidal cells in the barrel cortex of juvenile rats. J Physiol. 575:583–602.

Fox K. 1992. A critical period for experience-dependent synaptic plasticity in rat barrel cortex. J Neurosci. 12:1826–1838.

Galuske RA, Singer W. 1996. The origin and topography of long-range intrinsic projections in cat visual cortex: a developmental study. Cereb Cortex. 6:417–430.

Gilbert CD, Wiesel TN. 1979. Morphology and intracortical projections of functionally characterised neurones in the cat visual cortex. Nature. 280:120–125.

Gilbert CD, Wiesel TN. 1983. Clustered intrinsic connections in cat visual cortex. J Neurosci. 3:1116–1133.

Gilbert CD, Wiesel TN. 1989. Columnar specificity of intrinsic horizontal and corticocortical connections in cat visual cortex. J Neurosci. 9:2432–2442.

Glazewski S, Fox K. 1996. Time course of experience-dependent synaptic potentiation and depression in barrel cortex of adolescent rats. J Neurophysiol. 75:1714–1729.

Glazewski S, McKenna M, Jacquin M, Fox K. 1998. Experience-dependent depression of vibrissae responses in adolescent rat barrel cortex. Eur J Neurosci. 10:2107–2116.

Gonzalez-Burgos G, Barrionuevo G, Lewis DA. 2000. Horizontal synaptic connections in monkey prefrontal cortex: an in vitro electrophysiological study. Cereb Cortex. 10:82–92.

Gordon JA, Stryker MP. 1996. Experience-dependent plasticity of binocular responses in the primary visual cortex of the mouse. J Neurosci. 16:3274–3286.
Gottlieb JP, Keller A. 1997. Intrinsic circuitry and physiological properties of pyramidal neurons in rat barrel cortex. Exp Brain Res. 115:47–60.
Grinvald A, Lieke E, Frostig RD, Gilbert CD, Wiesel TN. 1986. Functional architecture of cortex revealed by optical imaging of intrinsic signals. Nature. 324:361–364.
Hoffer ZS, Arantes HB, Roth RL, Alloway KD. 2005. Functional circuits mediating sensorimotor integration: quantitative comparisons of projections from rodent barrel cortex to primary motor cortex, neostriatum, superior colliculus, and the pons. J Comp Neurol. 488:82–100.
Hoffer ZS, Hoover JE, Alloway KD. 2003. Sensorimotor corticocortical projections from rat barrel cortex have an anisotropic organization that facilitates integration of inputs from whiskers in the same row. J Comp Neurol. 466:525–544.
Hoover JE, Hoffer ZS, Alloway KD. 2003. Projections from primary somatosensory cortex to the neostriatum: the role of somatotopic continuity in corticostriatal convergence. J Neurophysiol. 89: 1576–1587.
Hu B, Nikolakopoulou AM, Cohen-Cory S. 2005. BDNF stabilizes synapses and maintains the structural complexity of optic axons in vivo. Development. 132:4285–4298.
Hubel DH, Wiesel TN, LeVay S. 1977. Plasticity of ocular dominance columns in monkey striate cortex. Philos Trans R Soc Lond B Biol Sci. 278:377–409.
Issa NP, Trachtenberg JT, Chapman B, Zahs KR, Stryker MP. 1999. The critical period for ocular dominance plasticity in the Ferret's visual cortex. J Neurosci. 19:6965–6978.
Kandel ER, Jessell TM, Sanes JR. 2000. Sensory experience and the fine tuning of synaptic connections. In: Kandel ER, Schwartz JH, Jessell TM, editors. Principle of neural science. New York: McGraw-Hill. p. 1115–1130.
Katz LC. 1999. What's critical for the critical period in visual cortex? Cell. 99:673–676.
Kenan-Vaknin G, Ouaknine GE, Razon N, Malach R. 1992. Organization of layers II-III connections in human visual cortex revealed by in vitro injections of biocytin. Brain Res. 594:339–342.
Kossut M. 1998. Experience-dependent changes in function and anatomy of adult barrel cortex. Exp Brain Res. 123:110–116.
Kossut M, Juliano SL. 1999. Anatomical correlates of representational map reorganization induced by partial vibrissectomy in the barrel cortex of adult mice. Neuroscience. 92:807–817.
Larsen DD, Callaway EM. 2006. Development of layer-specific axonal arborizations in mouse primary somatosensory cortex. J Comp Neurol. 494:398–414.
Levitt JB, Yoshioka T, Lund JS. 1994. Intrinsic cortical connections in macaque visual area V2: evidence for interaction between different functional streams. J Comp Neurol. 342:551–570.
Liposits Z, Sherman D, Phelix C, Paull WK. 1986. A combined light and electron microscopic immunocytochemical method for the simultaneous localization of multiple tissue antigens. Tyrosine hydroxylase immunoreactive innervation of corticotropin releasing factor synthesizing neurons in the paraventricular nucleus of the rat. Histochemistry. 85:95–106.
Livingstone MS, Hubel DH. 1983. Specificity of cortico-cortical connections in monkey visual system. Nature. 304:531–534.
Livingstone MS, Hubel DH. 1984. Specificity of intrinsic connections in primate primary visual cortex. J Neurosci. 4:2830–2835.
Lois C, Hong EJ, Pease S, Brown EJ, Baltimore D. 2002. Germline transmission and tissue-specific expression of transgenes delivered by lentiviral vectors. Science. 295:868–872.
Lübke J, Roth A, Feldmeyer D, Sakmann B. 2003. Morphometric analysis of the columnar innervation domain of neurons connecting layer 4 and layer 2/3 of juvenile rat barrel cortex. Cereb Cortex. 13:1051–1063.
Lund JS, Yoshioka T, Levitt JB. 1993. Comparison of intrinsic connectivity in different areas of macaque monkey cerebral cortex. Cereb Cortex. 3:148–162.
Martin KA, Whitteridge D. 1984. Form, function and intracortical projections of spiny neurones in the striate visual cortex of the cat. J Physiol. 353:463–504.
Meyer MP, Smith SJ. 2006. Evidence from in vivo imaging that synaptogenesis guides the growth and branching of axonal arbors by two distinct mechanisms. J Neurosci. 26:3604–3614.
Miller B, Blake NM, Erinjeri JP, Reistad CE, Sexton T, Admire P, Woolsey TA. 2001. Postnatal growth of intrinsic connections in mouse barrel cortex. J Comp Neurol. 436:17–31.
Nauta WJ, Bucher VM. 1954. Efferent connections of the striate cortex in the albino rat. J Comp Neurol. 100:257–285.
Paxinos G, Watson C. 1998. The rat brain in stereotaxic coordinates. San Diego: Academic Press.
Peters A, Jones EG. 1984. Cerebral cortex. Vol. I: Cellular components of cerebral cortex. New York: Plenum Press.
Petersen CC, Grinvald A, Sakmann B. 2003. Spatiotemporal dynamics of sensory responses in layer 2/3 of rat barrel cortex measured in vivo by voltage-sensitive dye imaging combined with whole-cell voltage recordings and neuron reconstructions. J Neurosci. 23: 1298–1309.
Petersen CC, Sakmann B. 2001. Functionally independent columns of rat somatosensory barrel cortex revealed with voltage-sensitive dye imaging. J Neurosci. 21:8435–8446.
Polley DB, Chen-Bee CH, Frostig RD. 1999. Two directions of plasticity in the sensory-deprived adult cortex. Neuron. 24:623–637.
Ratzlaff EH, Grinvald A. 1991. A tandem-lens epifluorescence macroscope: hundred-fold brightness advantage for wide field imaging. J Neurosci Methods. 36:127–137.
Rockland KS, Lund JS. 1983. Intrinsic laminar lattice connections in primate visual cortex. J Comp Neurol. 216:303–318.
Ruthazer ES, Li J, Cline HT. 2006. Stabilization of axon branch dynamics by synaptic maturation. J Neurosci. 26:3594–3603.
Shatz CJ, Stryker MP. 1978. Ocular dominance in layer IV of the cat's visual cortex and the effects of monocular deprivation. J Physiol. 281:267–283.
Simons DJ, Land PW. 1987. Early experience of tactile stimulation influences organization of somatic sensory cortex. Nature. 326: 694–697.
Stettler DD, Das A, Bennett J, Gilbert CD. 2002. Lateral connectivity and contextual interactions in macaque primary visual cortex. Neuron. 36:739–750.
Tanigawa H, Wang Q, Fujita I. 2005. Organization of horizontal axons in the inferior temporal cortex and primary visual cortex of the macaque monkey. Cereb Cortex. 15:1887–1899.
Trachtenberg JT, Stryker MP. 2001. Rapid anatomical plasticity of horizontal connections in the developing visual cortex. J Neurosci. 21:3476–3482.
Trachtenberg JT, Trepel C, Stryker MP. 2000. Rapid extragranular plasticity in the absence of thalamocortical plasticity in the developing primary visual cortex. Science. 287:2029–2032.
Wallace DJ, Sakmann B. 2007. Plasticity of representational maps in somatosensory cortex observed by in vivo voltage-sensitive dye imaging. Cereb Cortex. doi: 10.1093/cercor/bhm168.
Wirth C, Luscher HR. 2004. Spatiotemporal evolution of excitation and inhibition in the rat barrel cortex investigated with multielectrode arrays. J Neurophysiol. 91:1635–1647.
Wise SP, Jones EG. 1977a. Cells of origin and terminal distribution of descending projections of the rat somatic sensory cortex. J Comp Neurol. 175:129–157.
Wise SP, Jones EG. 1977b. Somatotopic and columnar organization in the corticotectal projection of the rat somatic sensory cortex. Brain Res. 133:223–235.
Yoshioka T, Levitt JB, Lund JS. 1992. Intrinsic lattice connections of macaque monkey visual cortical area V4. J Neurosci. 12:2785–2802.
Zaborsky L, Heimer L. 1989. Combination of tracer techniques, especially HRP and PHA-L, with transmitter identification for correlated light and electron microscopic studies. In: Heimer L, Zaborsky L, editors. Neuroanatomical tract tracing methods 2. New York: Plenum Press. p. 49–96.